# Current-rate flash sintering of gadolinium doped ceria: microstructure and defect generation

Tarini Prasad Mishra[a, b *] (ORCID ID: https://orcid.org/0000-0002-3176-5204)
Rubens Roberto Ingraci Neto[b] (ORCID ID: https://orcid.org/0000-0003-3064-9460)
Rishi Raj[b] (ORCID ID: http://orcid.org/0000-0001-8556-9797)
Olivier Guillon[a, c] (ORCID ID: http://orcid.org/0000-0003-4831-5725)
Martin Bram[a] (ORCID ID: http://orcid.org/0000-0002-1203-2777)

[a] Institute of Energy and Climate Research: Materials Synthesis and Processing (IEK-1),
Forschungszentrum Jülich GmbH, Jülich 52425, Germany
[b] Materials Science and Engineering Program, Department of Mechanical Engineering, University of Colorado Boulder, Boulder, Colorado
[c] Jülich Aachen Research Alliance, JARA-Energy, Germany

* Corresponding author. t.mishra@fz-juelich.de

IEK-1, Wilhelm-Johnen-Straße
52425 Jülich
Germany

## Abstract

In current-rate flash-sintering experiments the current is injected into the specimen from the very start and then increased at a constant rate, while the furnace is held at a constant temperature. The power supply remains under current control. The flash is induced at low current densities which reduces local heating at the electrodes. It leads to a uniform grain size across the entire gage length of the dog-bone specimen. This work pertains to 10 mol.% gadolinium-doped ceria flash sintered at current-rates ranging from 50 mA $min^{-1}$ to 1000 mA $min^{-1}$ at a furnace temperature of 680 °C. Full densities are obtained at a current density limit of 200 mA $mm^{-2}$. Densification is shown to depend only on the instantaneous value of the current density, and not on the current-rate. The grain size, however, is shown to become finer at higher current-rates. A preliminary analysis of the "energy deficit", that is, the estimated power input corresponding to the temperature as measured with a pyrometer, and the actual power consumption, estimates that huge concentrations of Frenkel defects may be introduced in the flash process.

*Keywords:* Current-rate Flash sintering, Flash Sintering, grain size, Frenkel pairs, Gadolinium-doped ceria

Shrinkage as a (i) function of time and (ii) function of the current density at different current rates

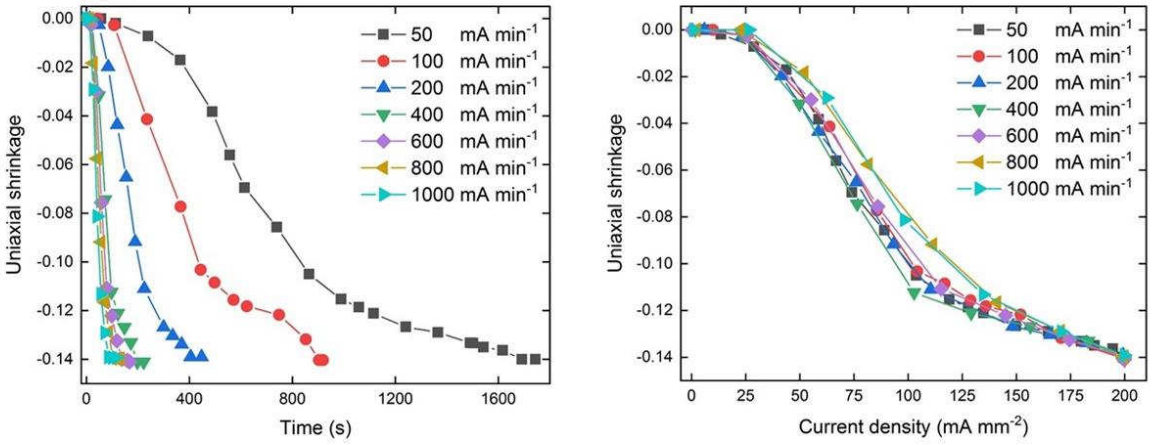


Graphical Abstract

## 1. Introduction

The first experiments in flash sintering were carried out by applying a constant electric field and then heating a dog-bone shaped, powder pressed sample of 3 mol% yttria stabilized zirconia (3YSZ), with a conventional furnace [1]. Flash was signaled by abrupt sintering to near full density, non-linear rise in conductivity, and by electroluminescence [2-5].

The above experiments are also done by holding the furnace temperature constant and applying the field as a step function. After an incubation time (referred to as Stage I) an abrupt rise in conductivity ~~(referred to as Stage I)~~ signals the flash event. The conductivity is limited by switching the power supply to current control (Stage II). The specimens can then be held in a steady state of flash under current control (Stage III) [3]. Under current control the voltage expressed across the specimen drops relative to the initial applied field, reflecting the higher conductivity of the specimen in a state of flash. These methods are called voltage-to-current experiments.

In 2018 [6] it was discovered that the flash experiment can be carried out by holding the specimen at a certain temperature (e.g. typically 900 °C for 3YSZ), and injecting current at a constant rate, with the power supply remaining under current control. The voltage developing

across the specimen was measured continuously. The transition to high conductivity was now expressed by a peak in the voltage profile. Continued increase in the applied current caused the voltage to change according to the change in the conductivity of the specimen. The temperature of the specimen increased with the current flowing through the specimen.

The current-rate experiments [6] yielded the following interesting outcomes

(i) Sintering occurred continuously with the increasing current, reaching full density at current densities that were similar to those in voltage-to-current experiments [3].

(ii) Remarkably the sinter density correlated with the instantaneous value of the current density. It was independent of the current-rate, even though the rate was increased over a factor of 100.

(iii) In voltage-to-current experiments the grain size distribution across the gage section of dog-bone specimens encumbers significant variability [7, 8]. In current-rate experiments, the grains size was uniform across the full gage section of the specimens. The present study is consistent with literature where it was shows that the grain size becomes finer at higher current-rates [9].

In the present work we report results from current-rate flash sintering experiments on 10 mol. % gadolinium-doped ceria, referred to as GDC. This ceramic is a mixed ionic and electronic conductor; it belongs to the rare earth doped ceria group. These ceramics hold promise for use in electrochemical devices such as gas separation membranes, solid oxide fuel cells, and solid oxide electrolysis cells. Among ceria-based ceramics, GDC possesses one of the highest ionic conductivity below 800°C [10, 11].

Conventional sintering of GDC usually requires several hours at 1400° C to 1600° C to achieve full density [12, 13]. Thus, flash sintering holds the promise of sintering GDC ceramics at low temperatures in short periods of time. Indeed, voltage-to-current experiments have been used to sinter GDC to full density quickly at 500-700°C [14-16]. However, the microstructure from these voltage-to-current experiments have not been reported. Therefore, as a precursor to the current-rate experiments, we

measured the grain size across the specimen in voltage-to-current experiments with GDC; the microstructure was, indeed, highly inhomogeneous.

The current-rate experiments were carried out on 10 mol. % gadolinium-doped ceria with a direct current (DC) power supply. The current density was varied over a factor of twenty from 50 to 1000 mA $min^{-1}$. The furnace was held at a constant temperature of 680 °C. In all instances full density was achieved at a current limit of 200 mA $mm^{-2}$. We show that the grain size can be controlled by changing the current-rate.

## 2. Experimental Methods and Materials

Commercial 10 mol.% gadolinium-doped ceria ($Gd_{0.10}Ce_{0.90}O_{1.95}$) powder (Fuel Cell Materials) with a particle size of $d_{10}$=0.07 μm, $d_{50}$=0.13 μm, $d_{90}$=1.97 μm, with a specific surface area of 10.5 $m^2/g$ (measured by Area Meter II, Ströhlein). The particle size distribution was measured by the laser diffraction method (LA-950-V2, Horiba Ltd., Tokyo, Japan). The particle size distribution and scanning electron microscopic images of the powder are included in Supplementary Materials as Fig S1. The average particle size was ~100 nm. The presence of large agglomerates in the range of 1-10 μm was noted.

The powder was mixed with a 2 wt% binder (Duramax B-1000 binder) and pressed uniaxially in a die to the shape of a dog-bone under a pressure of 100 MPa. These dog-bones had a gage length of 15 mm, a width of 3.3 mm, and a thickness between 1.95±0.15 mm. The amount of powder used for these specimens was 1.0±0.1 g. The green body samples were too fragile to connect to the electrodes. Therefore, they were heated to 600° C for 1 hour to remove the binder, and then pre-sintered at 1000°C for 30 minutes with a heating and cooling ramp of 3 K $min^{-1}$. The density of the pre-sintered samples, measured from the weight and the physical dimensions, was approximately 62.5%.

These green specimens were connected to a pair of platinum wires wrapped through the holes in the ears of the dog-bones. Platinum paste was applied for good electrical contact. The specimen was hung with the platinum wires into the hot-zone of a tubular vertical furnace, similar to the experimental set-up shown in [17]. Electrical power was fed to the specimen from a Sorensen DLM 300-2 (AMETEK Programmable Power, San Diego, CA, USA) power source. The current was measured with a digital multi-meter

(Keithley 2000, Keithley Instruments, Cleveland, OH). The communication and control of the power supply was achieved by DAQ USB-6008 (National Instruments). The GPIB was used to communicate with the multimeter, the device that monitors the current. Data was acquired through a graphical user interface (GUI) developed in-house at Boulder, running on the MATLAB platform. The voltage expressed across the specimen was measured at the power supply. The power consumed in the sample (per unit volume) was calculated as the product of current density and the electric field. The sample shrinkage was recorded through a digital camera with optical filters placed at the bottom of the furnace. The linear shrinkage strain was calculated from these recorded images typically obtained at 1 second intervals.

All experiments were carried out at a constant furnace temperature of 680°C. The samples were placed within the furnace for 15 minutes before turning on the current. The current was increased at the following current-rates, 50, 100, 200, 400, 600, 800 and 1000 mA $min^{-1}$. In all instances the power to the specimen was stopped when the current density reached 200 mA $mm^{-2}$. In this way, the total time for the experiment ranged from about 1 minute to 28 min. The time, current density and current-rate are summarized in the Supplementary Table S1.

After flash sintering, the ear sections of the samples were removed carefully and only the gauge section was considered for characterization. The densities of the sintered samples were measured by the Archimedes' principle with distilled water as a liquid medium. The values for the relative densities were calculated assuming a theoretical density of 7.22 $g/cm^3$.

For microstructure, cross-sections of samples were polished according to the standard metallographic process. The surfaces were thermally etched by annealing at 1250 °C for 20 minutes, to reveal the grain boundaries. The specimens were sputter coated with platinum. The microstructures were imaged with a table-top SEM (Phenom, Fei Company, Oregon, USA). Average grain size of the sintered body was determined by the linear intercept method from at least 500 randomly selected grains for each measurement. Linecut for Matlab software was used to determine the average grain size from the SEM micrographs [18].

The pre-sintered and the flash sintered samples were analyzed by X-ray diffraction XRD (Bruker AXS GmbH, Karlsruhe, Germany) using Cu Kα

radiation. The operating voltage and current were 40 kV and 40 mA. The lattice parameters were determined using Pawley's method for the refinement with TOPAS software (Bruker Corporation, Germany). The average crystallite size of the samples were estimated by the X-ray line broadening technique performed on the (2 2 0) diffraction of the $CeO_2$ lattice from the Scherrer equation.

# 3. Results and Discussion

## 3.1. Electric Field, Power Density and Temperature

The voltage expressed across the specimen rises as the current is increased. The sudden rise in conductivity, a signature event for flash, is therefore signaled by a drop in the voltage; therefore, the maximum in the voltage curve identifies the onset of flash. This behavior for different current-rates is given in Fig. 1(a). The peaks in the voltage profiles are quite distinct in the range of current-rates from 200 to 1000 mA $min^{-1}$. At lower current-rates they are somewhat subdued but still discernible. In all instances the flash initiates at current densities in the range of 7-9 mA $mm^{-2}$.

In voltage to current experiments the onset of flash encumbers an incubation time which depends on the electrical field. A similar behavior is seen here. If the current-rate is $\dot{J}$ mA $mm^{-2}$ $min^{-1}$ and the current-density at the onset of flash (i.e. the peak in the voltage) is $J_{flash}$ mA $mm^{-2}$, then the incubation time is given by

$$t_{inc} = \frac{J_{flash}}{\dot{J}} \qquad (1)$$

A plot of the electric field at the peak (as measured from Fig. 1a) and the incubation time, as calculated from Eq. (1) are given in Fig. 1(b). The incubation time lengthens significantly at lower electric fields which is consistent with earlier work on voltage-to-current experiments[3] .

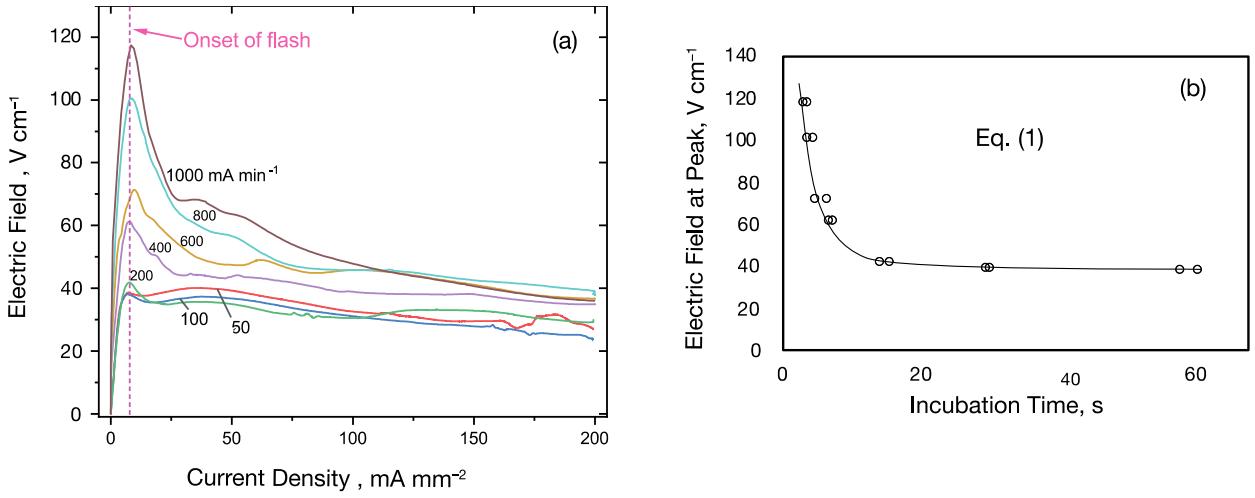


Fig. 1. (a) Electric field generated across the specimen when driven by different values of the constant current-rate. (b) The incubation time, given by the peak in the voltage profile, as a function of the value of the voltage at the peak.

The power consumption, per unit volume is given by

$$P_W = \rho J^2 \qquad (2)$$

where $\rho$ is the resistivity and $J$ is the current density. The curves for the power consumption as a function of current density are given in Fig. 2(a). They show a rise in power density but at a much lower rate than $J^2$, the implication being that the resistance declines with current density. The decline in resistance may be explained by the rise in temperature with current density. An increase in conductivity with temperature is consistent with ionic transport.

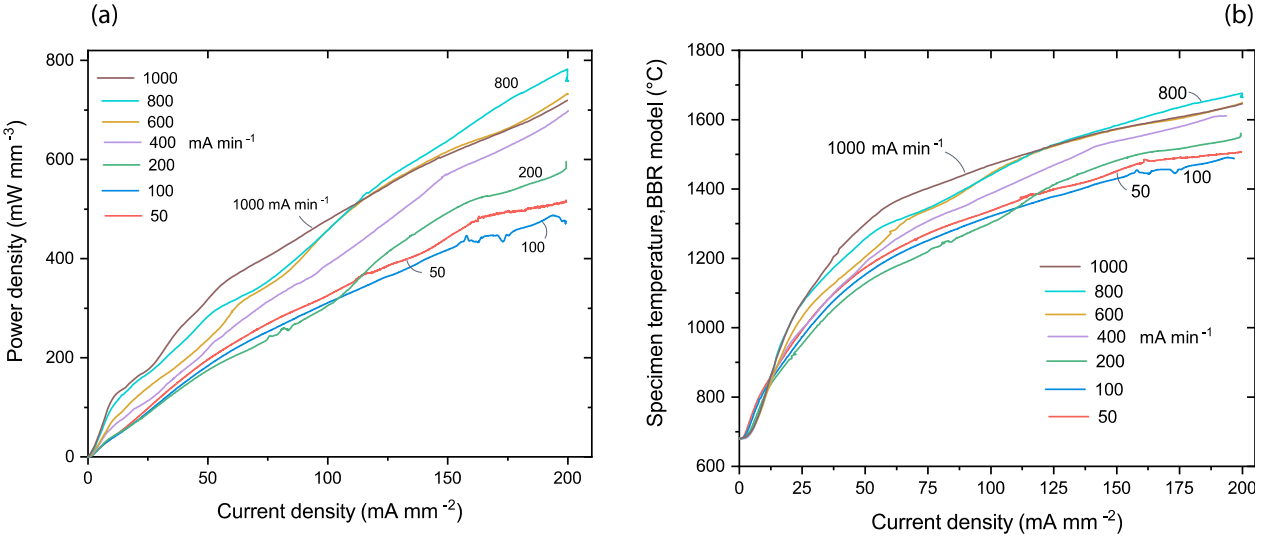

Fig. 2. (a) Power density as a function of the current density at different current rates. (b) Specimen temperature estimated from the black body radiation model as a function of the current density.

The specimen temperature during flash has been measured with a pyrometer and estimated by a black body radiation (BBR) model. In a steady state of flash (Stage III in voltage-to-current experiments) these two estimates match quite well not only with one another but also with direct measurements with a platinum standard during *in-situ* experiments at APS and BNL synchrotrons [22, 23]. These comparisons assumed the emissivity of zirconia to lie in the 0.8 to 1.0 range. The steady state BBR model assumes that the power consumption is equal to the radiation loss. However, the present situation is not steady state since the power consumption increases continuously with the current density; some of the input energy is, therefore, absorbed by specific heat.

In the original paper on current-rate experiments the steady state BBR model was amended to account for the energy stored as heat capacity when the specimen temperature changes [6]. Accordingly, the input power was equated to the sum of two terms as below

$$\int_t^{t+\Delta t} P_W dt = \int_t^{t+\Delta t} \omega_W(t)\, dt + \int_t^{t+\Delta t} \varphi_W(t,T) dt \qquad (3)$$

Here the total electrical power spent in the specimen, $P_W$, given by the left hand side, is equated to the enthalpy absorbed in specific heat, $\omega_W$, and the energy lost to black body radiation, $\varphi_W$. The complete analysis for this amended BBR model is given in [6]. The model was applied to the current experiments assuming the emissivity of GDC to be 0.9, and the specific heat to be 900 J $kg^{-1}$ $K^{-1}$ as reported by Stelzer et. al for [24]. Note that the surface area of the specimen was updated continuously while the sample sintered.

The above results are shown as temperature vs. current density in Fig. 2(b). They range up to a current density of 200 mA $mm^{-2}$ which was the upper current limit placed on the experiments. In all instances the temperature rises with the current density. We note that (i) a higher temperature implies a lower resistivity – for ionic transport – but also that (ii) the temperature, as well as the power density are higher for faster current-rates, which, from Eq. (1), may imply that the resistance is increasing with temperature, which suggests some degree of metallic character. It is possible that the material becomes a mixed ionic and

electronic conductor in a state of flash, a result which has been discussed in recent papers [19-21].

## 3.2 X-ray and Grain Size

The XRD diffraction pattern showed that the flashed samples retained their original cubic fluorite structure. These X-ray data are included in Supplementary Materials in Fig. S2.

While there was significant grain growth during the sintering process – from about 60 nm to >200 nm – the hall mark of the current-rate experiment from present work, and from literature [6, 9, 25], is the uniformity of grain size across the full gage section. In contrast, in voltage-to-current experiments the grain size distribution is often inhomogeneous [7, 8].

The uniformity of the grain size in the present experiments is shown by the plot in Fig. 3, for the case of 50 mA $min^{-1}$. The plots include the grain size on the outer surfaces and from the middle core of the specimen. The grain size in the core is seen to be larger than on the surfaces. We explain this finding by a higher temperature in the core relative to the surfaces. Pereira da Silva et. al. studied the temperature distribution of 8YSZ by the finite element method [26] for voltage-to-current experiments. They found significantly higher temperature in the mid-section ~~section~~ of the sample as compared to the top and bottom surfaces, presumably because of radiative losses from the surface. Most likely the larger grain size in the core region is related to such higher temperature.

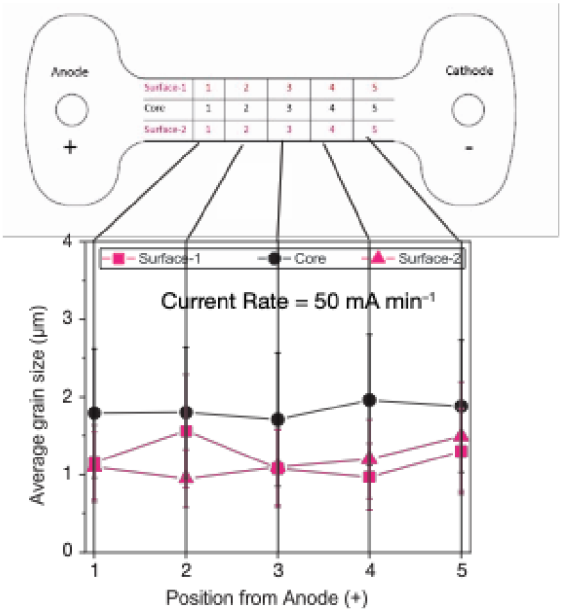


Fig. 3. Grain size at different locations along the gage length of the dog-bone specimens, at a current-rate of 50 mA $min^{-1}$.

The grain size micrographs from specimens flashed at different current-rates are shown in Fig. 4 (micrographs for other current-rates are included in Supplementary materials as Fig. S3). The micrographs on the left were obtained near the anode, and the ones on the right from near the cathode, and the one in the middle from the in-between region. The abnormal grain growth often seen near the electrodes in voltage-to-current experiments is absent. This result confirms this special feature of current-rate from earlier papers [6, 9, 25].

A possible explanation for this dichotomy between current-rate and voltage-to-current experiments is the great difference in the current density at the initiation of flash. In voltage-to-current experiments the current density rises nearly catastrophically to the current limit which is often in the range of 50 mA $mm^{-2}$ to 200 mA $mm^{-2}$. These high currents can produce large voltage drops at the electrodes - given by the product of the current density and the charge transfer interface resistance - which produces local heating. Furthermore, the voltage drops can be large enough to produce redox reactions which can exacerbate the local heating particularly for the reduction reaction at the cathode.

In contrast, in the current-rate experiments the current density at the onset of flash, as shown in Fig. 1 was in the 7-9 mA $mm^{-2}$ range, which may reduce the voltage drop across the interface thereby sidestepping the reduction reaction.

(The relationship between electroreduction and non-uniform grain size, however, has yet to be clearly established. Jha et al. [27] have reported abnormal lattice expansion near the cathode, measured by in-situ X-ray diffraction which was attributed to the accumulation of oxygen vacancies. Similar electro-reduction has been observed in 8 mol% yttria stabilized zirconia [28]. The link to grain growth remains unresolved.

As a benchmark we conducted a voltage-to-current experiment as a precursor to the current-rate experiments and found the grain size to be highly variable, being 3±1.1 µm near the anode, 0.70±0.35 µm in the center and 0.40±0.23 µm at the cathode; as seen in Fig. S4 in Supplementary Material.)

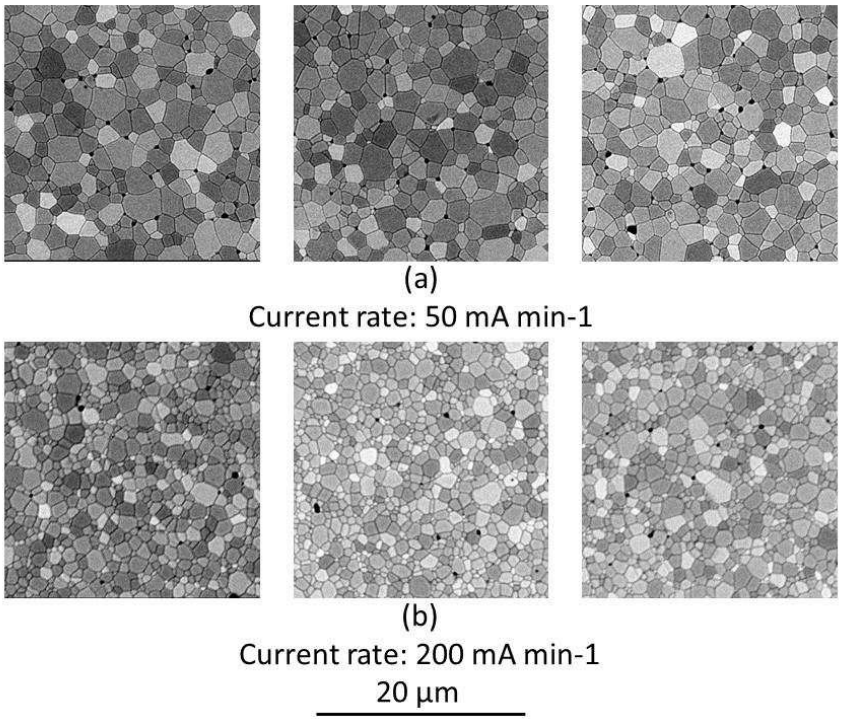

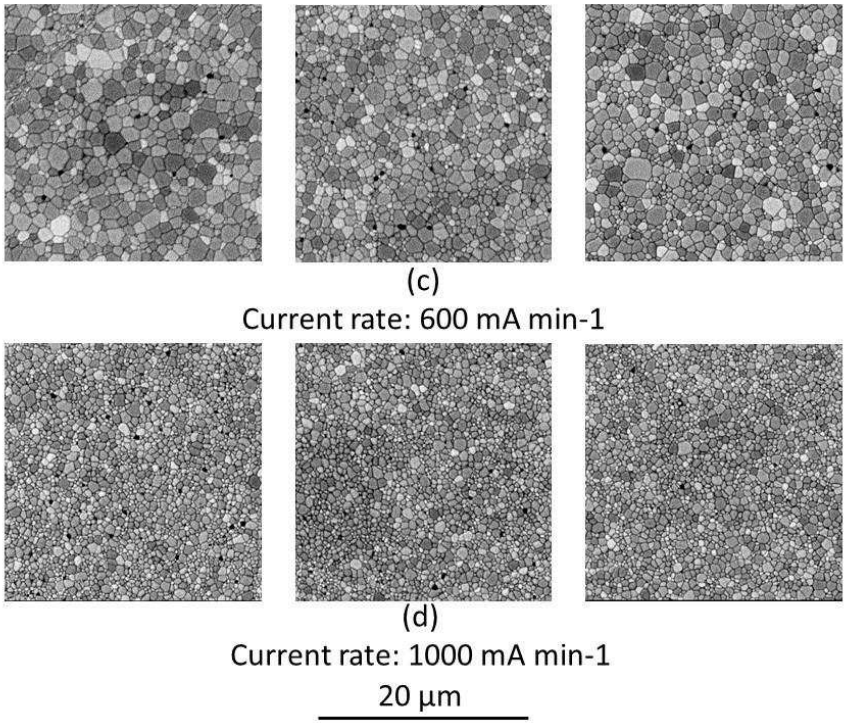


Fig. 4. SEM micrographs from near the anode (on the left), the middle, and the cathode (on the right), at different current-rates, (a) 50 mA $min^{-1}$, (b) 200 mA $min^{-1}$, (c) 600 mA $min^{-1}$ and (d) 1000 mA $min^{-1}$. Note the finer grain size at higher current rates.

Returning to Fig. 4, we note that the grain size changes with the current-rate. A plot of the grain size vs. current-rate is given in Fig. 5. The grain size decreases from ~3 µm at 50 mA $min^{-1}$ down to ~0.5 µm at 1000 mA $min^{-1}$. These results are different from earlier current-rate experiments with 3YSZ where the grain size was seen to remain unchanged with current-rates. However, the present results are consistent with other results from the literature [9].

As shown in the next section the extent of sintering was independent of the current-rate. The result that the grain size varies with current rate, but sintering does not, may suggest that grain growth and sintering are controlled by different mechanisms in flash experiments.

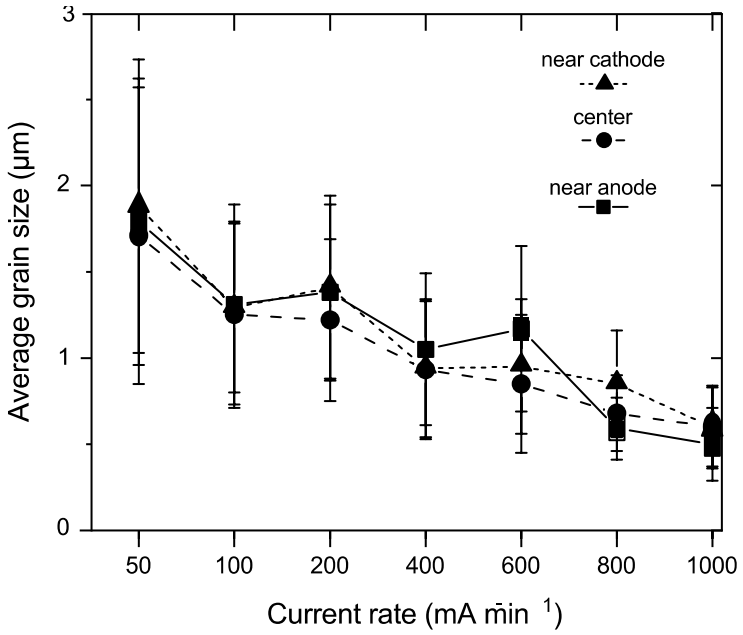


Figure 5. The grain size distribution across the gage length at different current-rates.

## 3.3 Sintering

One remarkable result from the first set of systematic current-rate experiments [6] was that densification depended only on the instantaneous value of the current density; it was independent of the current-rate.

The shrinkage strain was measured continuously ~~rate~~ from photographs taken at 1 s intervals. The linear shrinkage strain, $\varepsilon$, is given by

$$\varepsilon = \ell n\left(\frac{L}{L_o}\right) \qquad (4)$$

Where $L_0$ and $L$ are the initial and the time dependent gage lengths. Note that the strain is a negative quantity.

The shrinkage strain is plotted as a function of the instantaneous values of the current density in Fig. 6(a), and against the time for all current-rates in 6(b). It is quite remarkable, but in agreement with earlier work [6], that densification is independent of the current-rate – it depends only on the current density. While scientifically fascinating, this result also has practical value. In the voltage-to-current experiments sintering occurs in just a few seconds which makes it difficult to obtain *in-situ* experimental data, for example in live X-ray experiments. But current-rate experiments can stretch out the shrinkage to

several minutes simply by slowing down the current-rate. ~~These experiments are therefore become amenable for scientific studies.~~

Linear shrinkage is related to the change in relative density by [29]

$$\ell n\left(\frac{\rho}{\rho_g}\right)=3\varepsilon \qquad (5)$$

assuming that the shrinkage is isotropic, which is supported by experiments with dog-bone specimens where shrinkage strains in the length, width, and thickness directions have been shown to be equal [30]. Further confirmation is obtained by comparing the final density calculated from Eq. (5) with the final density measured by the Archimedes' method. The numbers are as follows, $\rho_g$=0.62, the final linear shrinkage is 0.1425, which gives the finish density to be 95.6±0.45%. The Archimedes' density measured with distilled water as a liquid medium was 96%, assuming a theoretical density for GDC10 of 7.22 g/cm$^3$. The relative density values of all current control flash sintered specimens are summarized in the Supplementary Table S2.

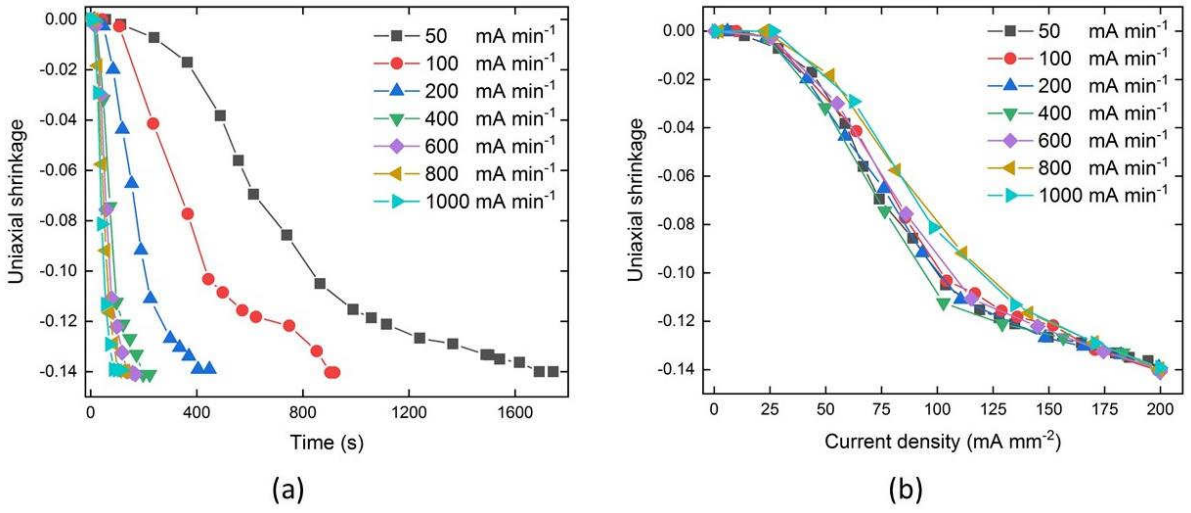


Fig. 6. (a) Variation of shrinkage as a function of real time for GDC10 at different current-rates, (b) Shrinkage as a function of current density for different current-rates

## 3.4 The Energy Deficit

Jean-Marie Lebrun, who contributed greatly to flash research in our laboratory used to say that in current-rate experiments the pyrometer temperature was often lower than the temperature estimated from the black

body radiation model. The systematic experiments in the present work permitted us to explore that observation rigorously.

We start by reiterating the key differences between voltage-to-current and current-rate experiments

(i) In voltage-to-current experiments sintering occurs quickly during the transition from voltage control to current control. Then, under current control the sample continues to flash in a steady state, such that the radiation loss is equal to the power consumption. In such a steady state the result from the BBR model has been shown to match the temperature measured with the platinum standard [31]. It is inferred that in voltage-to-current experiments a steady state of flash implies that the rate of defect generation equal to the rate of recombination.

(ii) The current-rate experiments have a fundamentally different texture; sintering occurs continuously as the current density is increased. The rate of sintering can be stretched out by slowing the current-rate. If indeed excess defects are the reason for flash sintering then these excess defects are being produced continuously.

The generation of defects is an endothermic process; therefore, it is possible that a portion of the power input is consumed in defect generation, with the rest being lost to radiation.

The analysis is approached by comparing the actual electrical power consumption, to the energy input that would be enough to account for the temperature measured with a pyrometer according to the BBR model. The difference then is the energy deficit which can be translated into excess defect concentration.

The analysis is given below. We specify the electrical power consumption as $W(t)$, in Watts, and the power that can account for the temperature measured with the pyrometer as $W^*(t)$. The energy deficit, as a function of time is then given by

$$\Delta H^*(t) = \int_0^t (W(t) - W^*(t))dt \qquad (5)$$

$\Delta H^*$ is in units of Joules and refers to the physical specimen. It is useful to convert it into per mole, as follows

$$\Delta H^*_{mol} = \frac{\Delta H^*}{V_{spec}/V_{molar}} \qquad (6)$$

Here $V_{spec}$ refers to the volume of the matter in the specimen and $V_{molar}$ is the molar volume of GDC. The molar volume is $V_{molar} = 2.36*10^4$ mm$^3$. The specimen volume, equal to the weight of the specimen divided by the density of ceria, was equal to $V_{spec} = 61.4$ mm$^3$. Thus, $\Delta H^*_{mol}$ is equal to the energy deficit per mole of GDC.

If the enthalpy of formation per one mole of Frenkel pairs is $\Delta H_{Fr}$, then the mole fraction of defects, $x_{Frenkels}$ created in the GDC is given by

$$x_{Frenkels} = \frac{\Delta H^*_{mol}}{\Delta H_{Fr}} \qquad (7)$$

It remains now to calculate $W^*(t)$ in Eq. (5). It is related to the pyrometer temperature (which we write as $T_K^p(t)$) through the BBR model[32], plus the heat absorbed in specific heat, so that

$$W^*(t) = \varepsilon_m S\sigma\left(\left[T_K^p\right]^4 - T_F^4\right) + mC_p\frac{dT_K^p}{dt} \qquad (8)$$

Here $S$ is the surface area of the specimen; it is corrected with time as the specimen shrinks. $\sigma$ is the Stephan Boltzmann's constant, and $\varepsilon_m$ is the emissivity. The furnace temperature is $T_F$, $m$ is the mass of the specimen, equal to 0.443 g. and $C_p$ is the specific heat, equal to 900 J kg$^{-1}$ K$^{-1}$ [24]. The nominal value for the emissivity of GDC is 0.8-1.0. We note that higher value of the emissivity increases $W^*$ and therefore decreases the energy deficit. Thus we set $\varepsilon = 1$ which gives the lower bound for the energy deficit.

To calculate the enthalpy of formation of one mole of Frenkels is sum of two anions and one cation. The enthalpy for one anion is 3.2 eV and 15.9 eV for the cation, for a total of 22.3 eV for two anions and one cation, which translates into $\Delta H_{Fr}$ = 2150 kJ mol$^{-1}$ of Frenkels.

Plots of $W$ and $W^*$ (for the case of 1000 mA min$^{-1}$) are given in Fig. 7(a), and the mole fraction of Frenkels calculated as above are given in

the upper curve in Fig. 7(b). The mole fraction of Frenkels rises to very large values, in the range of 20-30 mol%. If we assume that the pyrometer is underestimating the specimen temperature by 100 °C (the prediction from the BBR model has been shown to predict the measurements with a platinum standard to within $\pm 25$ °C) then the lower curve is obtained. Even then the Frenkel concentrations are more than 10%. These are very large numbers. We present these results with caution but with some confidence that the energy deficits as described here are factual.

The concentration of Frenkels calculated above are those that survive; they exclude those defects that recombine to return the enthalpy they consumed when they were formed. However, these surviving Frenkels can be absorbed in other ways, for example in the sintering process, by the vacancies becoming incorporated into grain boundaries, and the interstitials into the pores. (While the shrinkage of the pores does reduce free energy of the system, its magnitude is much smaller than measured here; and the energy of the grain boundaries is unlikely to change by absorption of vacancies). It is therefore possible that the large Frenkel concentrations we calculate are simply equal to those absorbed into the sintering process. Further experiments with dense polycrystals and single crystals are needed to clarify this point.

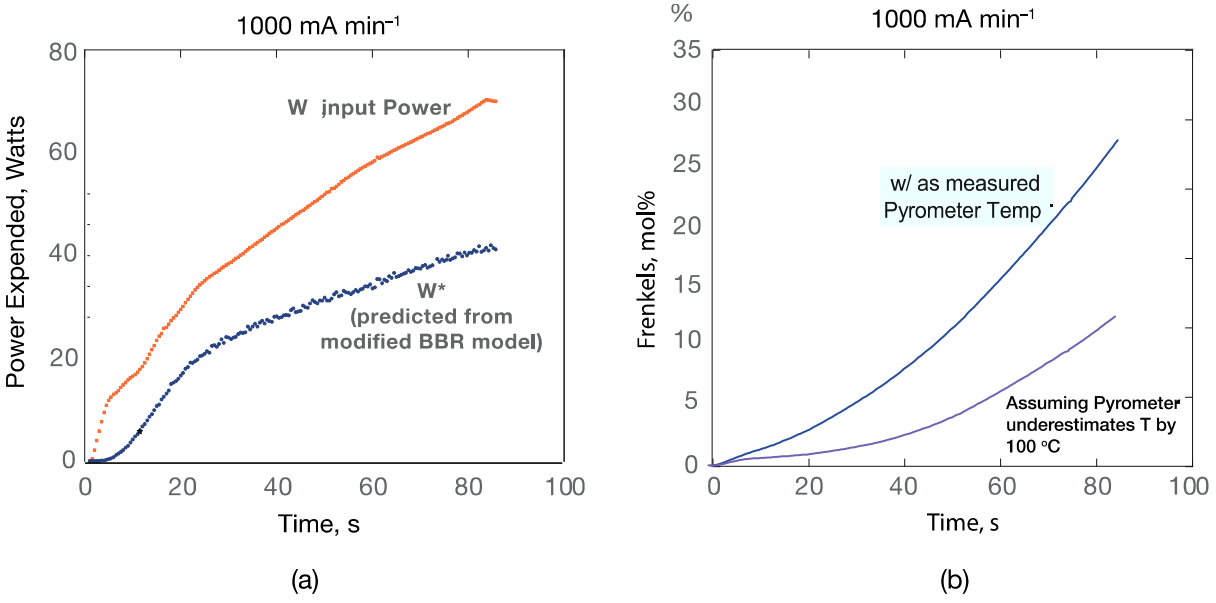


Figure 7. (a) Energy deficit as given by Eq. (5). (b) Mole fraction of Frenkel pairs estimated from the energy deficit, as given by Eq. (7).

It is possible that the energy deficit is not simply to be accounted for by Frenkels. There can be other endothermic reactions such as phase transformations that are far from equilibrium. Indeed new phases and heavy distortions in the X-ray diffraction peaks [33], and large atom displacements measured by pair distribution function analysis of total X-ray scattering data from Brookhaven [22] are examples of such events. It is conceivable that the defect generation is the precursor to the genesis of these unusual effects.

In closing we note the recent molecular dynamics simulations by Jongmanns and Wolf [34, 35] that point us to the endothermic nature of Frenkel pairs. In these simulations Frenkels were generated by the proliferation of phonons in a single crystal. The simulations were adiabatic that is, all the phonon energy was consumed either to raise the crystal temperature or to generate Frenkels. Once the crystal temperature reached the Debye temperature, all the input energy was used for the creation of Frenkels. A discussion of the significance of the Debye temperature is discussed in the literatures [2, 36]

## 4. Conclusions

Current rate experiments are a new development in the field of flash sintering; in them the power supply is always held under current control while the current is increased at a constant rate. They have significant differences with respect to the usual voltage-to-current experiments, where the voltage is applied as a step function, and the power supply is switched to current control at the onset of the flash. In the current rate experiments the onset of flash is signaled by a maximum on the voltage expressed across the specimen, which occurs at current densities that are far lower than the current limits used in the voltage-to-current experiments.

In contrast to the voltage-to-current experiments, the grain size in current-rate experiments is highly uniform across the full gage section of the dog-bone specimens. The grain size decreases with the current rate during the experiment. The absence of non-uniform grain size is attributed to the low current density for the onset of flash which avoids local heating at the electrodes. The grain size control, both with respect to

uniformity and its dependence on current-rate has technological significance.

The present experiments confirm the earlier experiments with 3 mol% yttria stabilized zirconia, that densification depends only on the instantaneous value of the current density, that is, it is independent of the current rate. The current rates were varied over a factor of 20; in this way the period during which the sample sinters could be stretched from about 1.4 min to 28 min. The stretched time is an important development for characterizing the evolution of the structure and defect concentrations while the specimen sinters. In voltage-to-current experiments sintering occurs nearly instantaneously when the power supply is switched from voltage control to current control, rendering it quite difficult to garner information during densification.

The specimen temperature measured with a pyrometer corresponds to a far lower power dissipation, as predicted by the black body radiation model, than the electrical power injected into the specimen. For the present this energy deficit is attributed to the endothermic nature of defect generation. The estimate is that defects in the 10-30 mol% are produced. It is of course possible that other endothermic phenomena such as the formation of phases that are far from equilibrium are absorbing a part of this energy deficit.

Another explanation can be that these Frenkels are absorbed at grain boundaries and pores which produces sintering, which does not have a significant enthalpy ramification; experiments with dense polycrystals and single crystals are underway to explore this possibility. In either case, the defect generation is “huge” so that the defects must now be considered as species in their own right, in addition to the anions and cations, in the study of phase stability under flash conditions. It may produce events that are far from equilibrium.

## Acknowledgements

This work is financially supported by the German Research Foundation (DFG) within the Priority Program on “manipulation of matter controlled by an electric and magnetic field, SPP 1959 under the Grant No. BR 3418/1-1”. Raj gratefully acknowledges support for this work from the Office of Naval

Research under Grant No. N00014-18-1-2270. It is a pleasure to acknowledge valuable discussions with Dr. Jean-Marie Lebrun, now at St. Gobain Ceramics.

## References

[1] M. Cologna, B. Rashkova, R. Raj, Flash Sintering of Nanograin Zirconia in <5 s at 850°C: Rapid Communications of the American Ceramic Society, Journal of the American Ceramic Society. 93 (2010) 3556–3559. https://doi.org/10.1111/j.1551-2916.2010.04089.x.

[2] T.P. Mishra, V. Avila, R.R.I. Neto, M. Bram, O. Guillon, R. Raj, On the role of Debye temperature in the onset of flash in three oxides, Scripta Materialia. 170 (2019) 81–84. doi:10.1016/j.scriptamat.2019.05.030.

[3] J.S.C. Francis, R. Raj, Influence of the Field and the Current Limit on Flash Sintering at Isothermal Furnace Temperatures, Journal of the American Ceramic Society. 96 (2013) 2754–2758. doi:10.1111/jace.12472.

[4] J.-M. Lebrun, R. Raj, A First Report of Photoemission in Experiments Related to Flash Sintering, Journal of the American Ceramic Society. 97 (2014) 2427–2430. https://doi.org/10.1111/jace.13130.

[5] M. Biesuz, P. Luchi, A. Quaranta, A. Martucci, V.M. Sglavo, Photoemission during flash sintering: An interpretation based on thermal radiation, Journal of the European Ceramic Society. 37 (2017) 3125–3130. https://doi.org/10.1016/j.jeurceramsoc.2017.03.050.

[6] P. Kumar M K, D. Yadav, J.-M. Lebrun, R. Raj, Flash sintering with current rate: A different approach, Journal of the American Ceramic Society. (2018). https://doi.org/10.1111/jace.16037.

[7] Y. Zhang, J.-I. Jung, J. Luo, Thermal runaway, flash sintering and asymmetrical microstructural development of ZnO and ZnO–Bi2O3 under direct currents, Acta Materialia. 94 (2015) 87–100. https://doi.org/10.1016/j.actamat.2015.04.018.

[8] W. Qin, H. Majidi, J. Yun, K.V. Benthem, Electrode Effects on Microstructure Formation During FLASH Sintering of Yttrium-Stabilized Zirconia, Journal of the American Ceramic Society. 99 (2016) 2253–2259. doi:10.1111/jace.14234.

[9] H. Charalambous, S.K. Jha, K.H. Christian, R.T. Lay, T. Tsakalakos, Flash Sintering using Controlled Current Ramp, Journal of the European Ceramic Society. 38 (2018) 3689–3693. https://doi.org/10.1016/j.jeurceramsoc.2018.04.003.

[10] K. Eguchi, T. Setoguchi, T. Inoue and H. Arai, "Electrical properties of ceria-based oxides and their application to solid oxide fuel cells," Solid State Ionics, vol. 52, p. 165 – 172, 1992.

[11] H. Inaba and H. Tagawa, "Ceria-based solid electrolytes," Solid State Ionics, vol. 83, pp. 1-16, 1996.

[12] D. Ni, J. Glasscock, A. Pons, W. Zhang, A. Prasad, S. Sanna, N. Pryds and V. Esposito, "Densification of highly defective ceria by high temperature controlled re-oxidation," *Journal of the Electrochemical Society,* vol. 161, pp. 3072-3078, 2014.

[13] V. Esposito, D.W. Ni, Z. He, W. Zhang, A.S. Prasad, J.A. Glasscock, C. Chatzichristodoulou, S. Ramousse, A. Kaiser, Enhanced mass diffusion phenomena in highly defective doped ceria, Acta Materialia. 61 (2013) 6290–6300. https://doi.org/10.1016/j.actamat.2013.07.012.

[14] L. Spiridigliozzi, M. Biesuz, G. Dell'Agli, E. Di Bartolomeo, F. Zurlo, V.M. Sglavo, Microstructural and electrical investigation of flash-sintered Gd/Sm-doped ceria, J Mater Sci. 52 (2017) 7479–7488. https://doi.org/10.1007/s10853-017-0980-2.

[15] X. Hao, Y. Liu, Z. Wang, J. Qiao, K. Sun, A novel sintering method to obtain fully dense gadolinia doped ceria by applying a direct current, Journal of Power Sources. 210 (2012) 86–91. https://doi.org/10.1016/j.jpowsour.2012.03.006.

[16] T. Jiang, Z. Wang, J. Zhang, X. Hao, D. Rooney, Y. Liu, W. Sun, J. Qiao, K. Sun, Understanding the Flash Sintering of Rare-Earth-Doped Ceria for Solid Oxide Fuel Cell, Journal of the American Ceramic Society. 98 (2015) 1717–1723. https://doi.org/10.1111/jace.13526.

[17] M. Cologna, J.S. Francis, R. Raj, Field assisted and flash sintering of alumina and its relationship to conductivity and MgO-doping, Journal of the European Ceramic Society. 31 (2011) 2827–2837. doi:10.1016/j.jeurceramsoc.2011.07.004.

[18] Meister S. grain and particle analysis with line intersection method - File Exchange - MATLAB Central [Internet]. Mathworks.com. 2012 [cited 26 June 2019]. Available from: https://www.mathworks.com/matlabcentral/fileexchange/35203-grain-and-particle-analysis-with-line-intersection-method

[19] S. Jo, R. Raj, Transition to Electronic Conduction at the Onset of Flash in Cubic Zirconia, Social Science Research Network, Rochester, NY, 2019. https://papers.ssrn.com/abstract=3414705 (accessed July 30, 2019).

[20] N. Masó, A.R. West, Electronic Conductivity in Yttria-Stabilized Zirconia under a Small dc Bias, Chem. Mater. 27 (2015) 1552–1558. https://doi.org/10.1021/cm503957x.

[21] R. Kirchheim, On the mixed ionic and electronic conductivity in polarized yttria stabilized zirconia, Solid State Ionics. 320 (2018) 239–258. https://doi.org/10.1016/j.ssi.2018.03.014.

[22] B. Yoon, D. Yadav, R. Raj, E. Sortino, S. Ghose, P. Sarin, et al., Measurement of O and Ti atom displacements in TiO 2 during flash sintering experiments, Journal of the American Ceramic Society. 101 (2017) 1811–1817. doi:10.1111/jace.15375.

[23] K. Terauds, J.-M. Lebrun, H.-H. Lee, T.-Y. Jeon, S.-H. Lee, J.H. Je, et al., Electroluminescence and the measurement of temperature during Stage III of flash sintering experiments, Journal of the European Ceramic Society. 35 (2015) 3195–3199. doi:10.1016/j.jeurceramsoc.2015.03.040.

[24] N. Stelzer, J. Nölting, I. Riess, Phase Diagram of Nonstoichiometric 10 mol% Gd2O3-Doped Cerium Oxide Determined from Specific Heat Measurements, Journal of Solid State Chemistry. 117 (1995) 392–397. doi:10.1006/jssc.1995.1290.

[25] X.L. Phuah, H. Wang, H. Charalambous, S.K. Jha, T. Tsakalakos, X. Zhang, et al., Comparison of the grain growth behavior and defect structures of flash sintered ZnO with and without controlled current ramp, Scripta Materialia. 162 (2019) 251–255. doi:10.1016/j.scriptamat.2018.11.009.

[26] Pereira da Silva J, Lebrun J, Al-Qureshi H, Janssen R, Raj R. Temperature Distributions During Flash Sintering of 8% Yttria-Stabilized Zirconia. Journal of the American Ceramic Society. 2015;98(11):3525-3528.

[27] S.K. Jha, H. Charalambous, H. Wang, X.L. Phuah, C. Mead, J. Okasinski, H. Wang, T. Tsakalakos, In-situ observation of oxygen mobility and abnormal lattice expansion in ceria during flash sintering, Ceramics International. 44 (2018) 15362–15369. https://doi.org/10.1016/j.ceramint.2018.05.186.

[28] M. Biesuz, L. Pinter, T. Saunders, M. Reece, J. Binner, V. Sglavo, S. Grasso, Investigation of electrochemical, optical and thermal effects during flash sintering of 8YSZ, Materials 11 (7) (2018) 1214.

[29] R. Raj, Separation of Cavitation-Strain and Creep-Strain During Deformation, Journal of the American Ceramic Society. 65 (1982) C-46-C–46. https://doi.org/10.1111/j.1151-2916.1982.tb10397.x.

[30] F. Shikhar, A study on Flash Sintering and Related Phenomena in Titania and its Composites with Alumina, (2015)

[31] K. Terauds, J.-M. Lebrun, H.-H. Lee, T.-Y. Jeon, S.-H. Lee, J.H. Je, R. Raj, Electroluminescence and the measurement of temperature during Stage III of flash sintering experiments, Journal of the European Ceramic Society. 35 (2015) 3195–3199. https://doi.org/10.1016/j.jeurceramsoc.2015.03.040.

[32] R. Raj, Joule heating during flash-sintering, Journal of the European Ceramic Society. 32 (2012) 2293–2301. https://doi.org/10.1016/j.jeurceramsoc.2012.02.030.

[33] J. Lebrun, T.G. Morrissey, J.S.C. Francis, K.C. Seymour, W.M. Kriven, R. Raj, Emergence and Extinction of a New Phase During On–Off Experiments Related to Flash Sintering of 3 YSZ, Journal of the American Ceramic Society. 98 (2015) 1493–1497. https://doi.org/10.1111/jace.13476.

[34] M. Jongmanns, R. Raj, D.E. Wolf, Generation of Frenkel defects above the Debye temperature by proliferation of phonons near the Brillouin zone edge, New Journal of Physics. 20 (2018) 093013. doi:10.1088/1367-2630/aadd5a.

[35] M. Jongmanns, D.E. Wolf, Element-specific displacements in defect-enriched TiO 2 : Indication of a flash sintering mechanism, Journal of the American Ceramic Society. (2019). doi:10.1111/jace.16696.

[36] D. Yadav, R. Raj, Two unique measurements related to flash experiments with yttria-stabilized zirconia, Journal of the American Ceramic Society. 100 (2017) 5374–5378. https://doi.org/10.1111/jace.15114.

# Supplementary materials

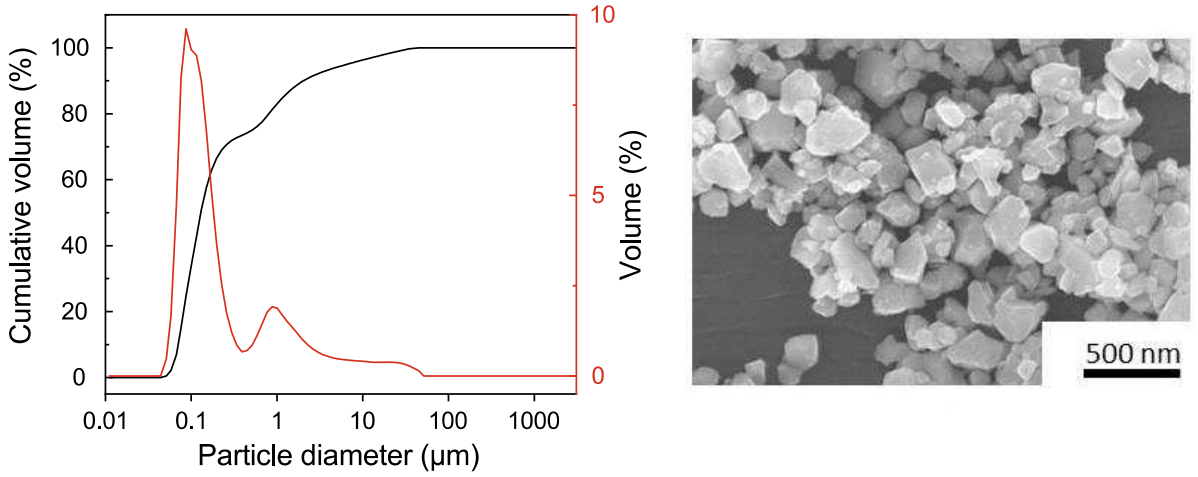


Supplementary Figure S1. (a) Particle size distribution of GDC10 powder, (b) SEM micrograph of GDC10 powder

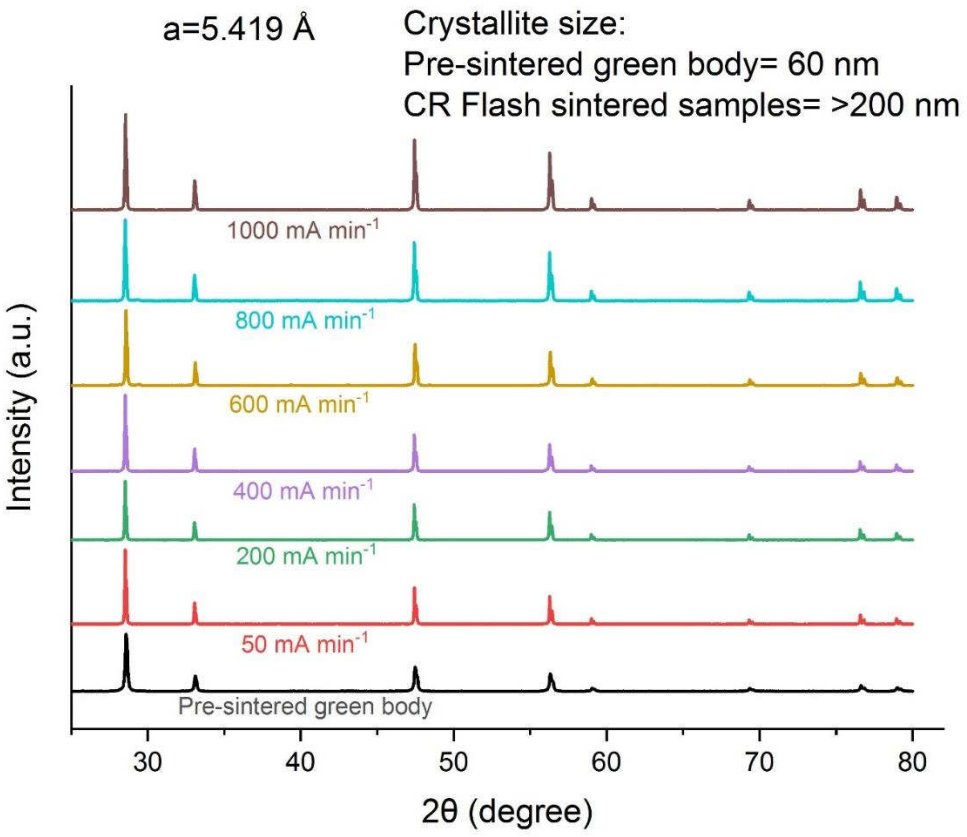


Supplementary Figure S2. X-ray diffraction of the starting specimen and CR flash sintered specimens showing the grain growth

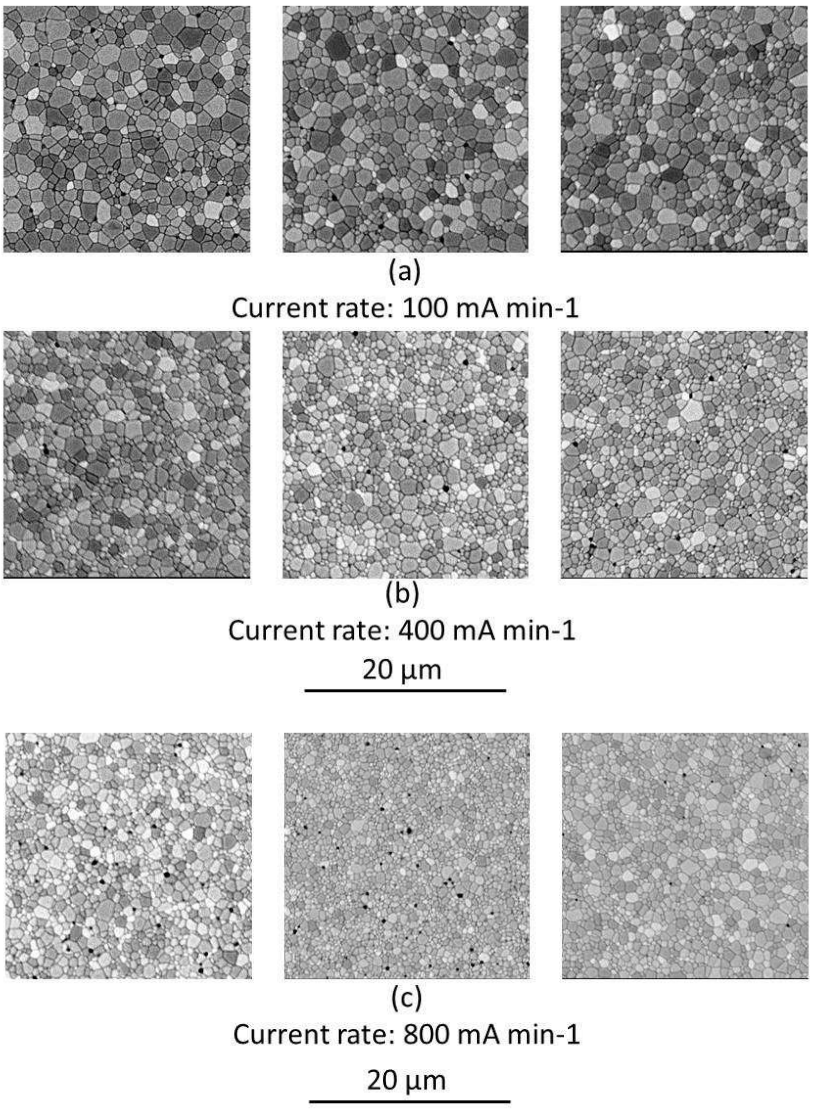


Supplementary Figure S3. SEM micrographs at three different positions (i.e. left image: near the anode, middle image: at the center of the sample and right image: near the cathode) of the CR Flash sintered samples at different current-rates, (a) 100 mA min-1, (b) 400 mA min-1 and (c) 800 mA min-1, showing higher current-rate resulted in finer grain size (homogeneous grain size distribution along the gauge section of the sample.

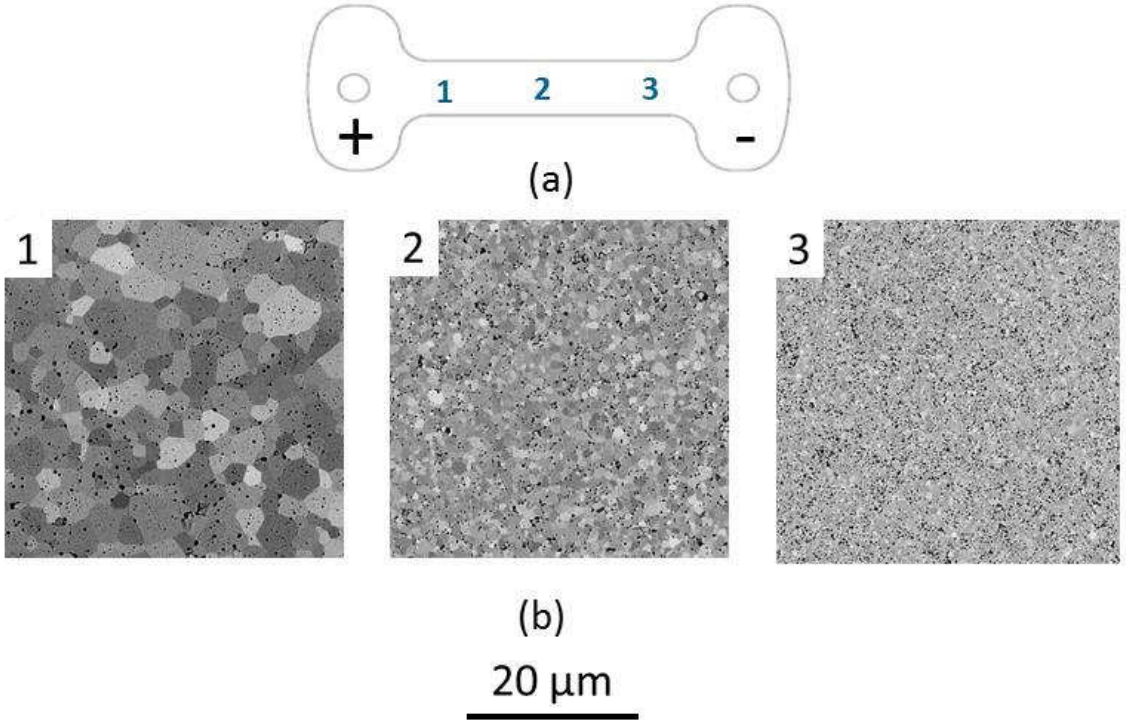


Supplementary Figure S4. (a) The locations between the electrodes where the SEM micrographs were taken. SEM micrographs comparing the microstructural differences near anode, center and near cathode for (b) voltage-to-current (applied field 150 $Vcm^{-1}$ and furnace temperature 680°C)

Supplementary Table S1: Total time of the experiment for different current-rate flash sintering experiments

| Experiment number | Current-rate (mA $mm^{-2}$) | Time for completion of the experiment (minutes) |
|---|---|---|
| 1 | 50 | 28 |
| 2 | 100 | 14 |
| 3 | 200 | 7 |
| 4 | 400 | 3.2 |
| 5 | 600 | 2.3 |
| 6 | 800 | 1.8 |
| 7 | 1000 | 1.3 |

Supplementary Table S2: Relative density of the current control flash sintered specimens measured by the Archimedes' method with distilled water as a liquid medium; the values for the relative densities were calculated assuming a theoretical density for GDC10 of 7.22 g/cm3.

| **Current-rate (mA $min^{-1}$)** | **Relative density (%)** |
|---|---|
| 50 | 95.88 |
| 100 | 95.62 |
| 200 | 95.17 |
| 400 | 96.36 |
| 600 | 95.7 |
| 800 | 94.74 |
| 1000 | 95.57 |